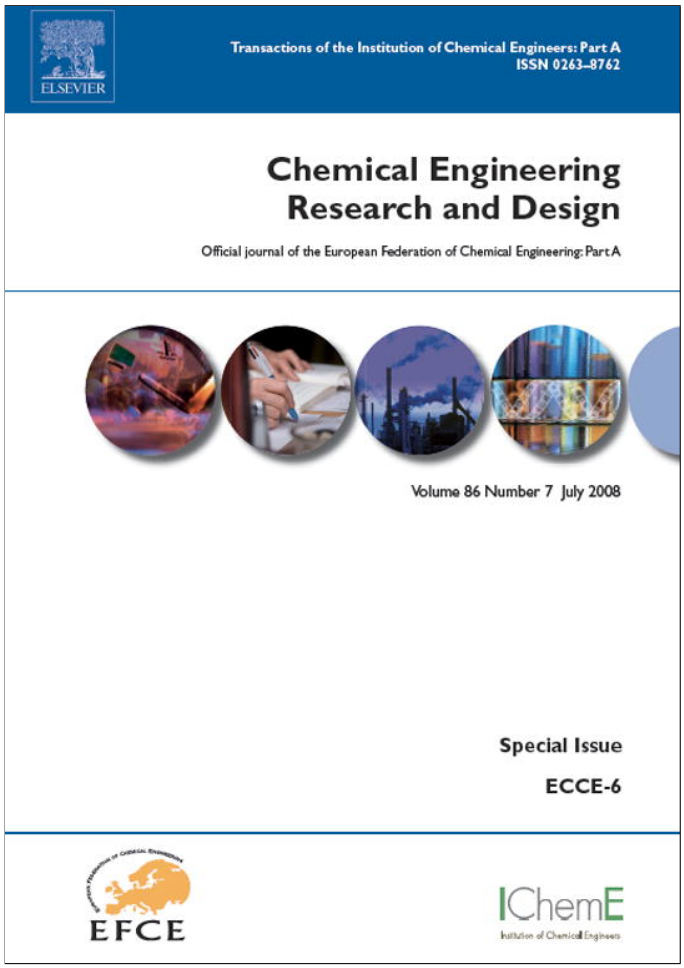

CHEMICAL ENGINEERING RESEARCH AND DESIGN 86 (2008) 739–744

available at www.sciencedirect.com

ScienceDirect

journal homepage: www.elsevier.com/locate/cherd

Viscous stabilization of drying front: Three-dimensional pore network simulations

Thomas Metzger, Evangelos Tsotsas*

Thermal Process Engineering, Otto-von-Guericke-University, P.O. 4120, D-39016 Magdeburg, Germany

ARTICLE INFO

Article history:
Received 24 October 2007
Accepted 9 March 2008

Keywords:
Capillary porous media
Phase distributions
Drying rate curves

ABSTRACT

In this study, a recently developed pore network drying model [Metzger, T., Irawan, A. and Tsotsas, E., 2007, Isothermal drying of pore networks: influence of friction for different pore structures, Dry Technol, 25: 49–57], which accounts for liquid viscosity, is applied to three dimensions for the first time. Isothermal convective drying is simulated for a cubic network ($25 \times 25 \times 50$) with pore throats with a narrow radius distribution. The role of liquid viscosity is assessed by comparison with non-viscous drying of the same network. Simulation results are presented as phase distributions, saturation profiles and drying rate curves. In the viscous case, a stabilization of the drying front is observed. However, as the network dries out from the surface, the finite drying front gradually widens up and does not approach an asymptotic limit.

1. Introduction

Pore network models are a suitable tool to examine the role of pore-scale transport phenomena and pore structure on the process behaviour of porous media. During the past one-and-a-half decades, several research groups have applied pore network modelling to drying of capillary porous media, continuously adding new transport phenomena and increasing network size.

In network models, the porous medium is represented by a network of interconnected pores which have a prescribed geometry (cylindrical in our study) but are random in their size. Our model approach is based on the work of Prat (1993) who interpreted the drying process as an invasion percolation driven by evaporation. At every moment of the process, the largest pore at the gas–liquid interface empties because its meniscus can produce the highest liquid pressure. Due to random spatial distribution of pore size, the liquid phase typically splits up into numerous clusters that may be temporarily trapped, but eventually all liquid will evaporate. The time scale of the process is given by vapour diffusion in the empty regions of the network.

In this isothermal model, capillary flow is only determined by the spatial distribution of pore size. However, if other effects like gravity, liquid viscosity or non-uniform temperature play a role, drying behaviour can differ significantly. The model extension to gravity is straightforward by allocating to each pore a potential which then determines the order of invasion (Prat, 1993). If the network dries out from the top, gravity has a stabilizing effect on the drying front. Laurindo and Prat (1996) performed experiments with two-dimensional micro models which nicely confirmed the simulated phase patterns as well as their modification due to gravity.

Recently, the stabilizing effect of gravity has also been studied in three dimensions by Yiotis et al. (2006) who simulated drying of an $80 \times 80 \times 80$ network. If gravity plays no role and lateral diffusion in the gas-side boundary layer is modelled, they found a constant drying rate period. Such computationally intensive three-dimensional network simulations are important, because the additional dimension leads to less trapping (see also Le Bray and Prat, 1999).

Prat and Bouleux (1999) predicted a stabilization of the drying front if liquid viscosity must be accounted for (i.e. for large networks of small pores with a narrow size distribution); however, they only performed stationary network simulations. Other researchers have included viscous effects into their (two-dimensional) pore network models, but the effect of liquid viscosity on drying kinetics and phase distributions has

* Corresponding author. Tel.: +49 391 6711362: fax: +49 391 6711160.
E-mail address: thomas.metzger@ovgu.de (T. Metzger).

0263-8762/$ – see front matter © 2008 The Institution of Chemical Engineers. Published by Elsevier B.V. All rights reserved.
doi:10.1016/j.cherd.2008.03.003

IChemE

never been studied systematically: Nowicki et al. (1992) were interested in effective parameters and did not report on phase distributions and drying rates at the sample scale; and Yiotis et al. (2001) simulated drying of porous rock when gas is purged through large fractures and viscous effects mainly play a role in the gas phase.

The stabilization of the gas invasion front in drying for gravity and liquid viscosity has also been characterized by scaling laws (Tsimpanogiannis et al., 1999; Prat and Bouleux, 1999); experimental data for the viscous stabilization had already been reported by Shaw (1987) for the drying of a bed of small glass spheres.

In the present work, we will study viscous stabilization of the front by a three-dimensional pore network drying model and discuss its effect on the drying rate curve. We will focus on the special character of this stabilization: whereas front width is constant throughout the drying process in the gravity-stabilized case, viscous effects depend on current flow rates so that the drying front can widen up during the process.

It is worth mentioning that temperature gradients will also lead to a stabilization of the drying front (Huinink et al., 2002; Plourde and Prat, 2003) if the open surface of the network is hotter—as in convective drying. The reason for this is temperature dependence of surface tension, so that out of two pores of identical radius the warmer one will empty first.

Another stabilization effect is obtained if the pores are not cylindrical but have corners so that gas-invaded pores may still contain corner films. Film flow, which is induced by capillarity and limited by liquid viscosity, has been modelled by Yiotis et al. (2003, 2004) and Prat (2007). The film region typically covers the liquid cluster region as well as part of the completely invaded region. As a result of film flow, the evaporation front is smoothened in space and shifted towards network surface, resulting in higher drying rates. Experimental evidence of film flows and their effect on drying kinetics has been given by Laurindo and Prat (1998).

In general, stabilization effects are seen as crucial if drying is to be described by a continuous model (see, e.g. Tsimpanogiannis et al., 1999). In non-stabilized percolation, drying front width has no upper limit, and continuum models lack their basis, namely gradient-based (liquid) transfer.

Besides this research on transport phenomena, an investigation of structural influences on drying behaviour has recently been started. Prat (2007) has studied the role of pore shape in the context of film flow; Segura and Toledo (2005) have investigated the role of pore shape and pore size distributions for drying behaviour and effective transport parameters; Metzger et al. (2007a) have shown that pore structures with a bimodal pore size distribution may show very different drying behaviour and that coordination number of the pore network and spatial correlations of pore size play a crucial role (Metzger et al., 2007b). In the present work, we will however restrict ourselves to isothermal drying of a network of cylindrical pores (i.e. without corner films) with mono-modal radius distribution.

2. Drying model

In the following, the main concepts of non-viscous and viscous network drying model are recalled (for more details refer to Metzger et al., 2007c).

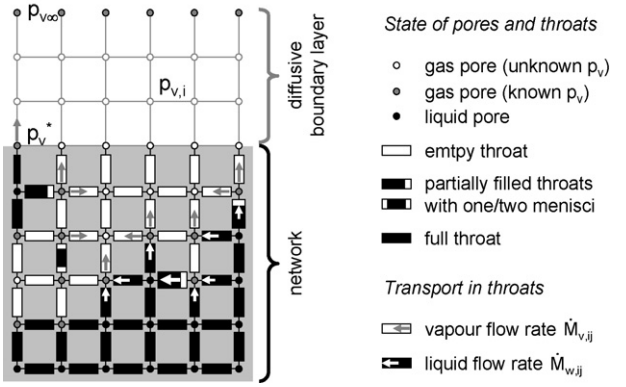

Fig. 1 – Small pore network during drying with discretized gas-side boundary layer. Definitions of pore and throat states are given; vapour and liquid transport are indicated.

2.1. Non-viscous model

The cubic pore network is built from cylindrical pore throats with radii r_{ij} obeying a normal number distribution. Initially, the network is fully saturated with water. During drying, it is open for evaporation at the top whereas the bottom is closed and the sides are connected for periodic boundary conditions in horizontal directions. Fig. 1 shows a small two-dimensional (non-periodic) pore network in the course of convective drying as a visual support for model description.

Vapour transfer to the dry air flow is modelled by diffusion through a boundary layer of uniform thickness which is discretized by extending the nodes of the network. In the gas phase (dry part of network and boundary layer), quasi-steady vapour diffusion between two nodes is described by

$$\sum_j \dot{M}_{v,ij} = \sum_j A_{ij} \frac{\delta}{L} \frac{\tilde{M}_v p}{\tilde{R}T} \ln\left(\frac{p - p_{v,i}}{p - p_{v,j}}\right) = 0 \quad (1)$$

where L is distance between nodes, A_{ij} exchange area (πr_{ij}^2 for network, L^2 for boundary layer), δ vapour diffusivity, $\tilde{M}_v$ molar vapour mass, $\tilde{R}$ universal gas constant, T absolute temperature, p gas pressure and $p_{v,i}$ vapour pressure. The system of Eq. (1) is solved to compute the unknown vapour pressures in the gas pores (white circles) by applying as boundary conditions the known vapour pressure (gray circles) of drying air $p_{v,\infty}$ at the top edge of the boundary layer and saturation vapour pressure p_v^* in pores next to the gas–liquid interface. From this, vapour diffusion rates can be computed for the empty throats (white rectangles) and evaporation rates for the menisci at the liquid–gas interface.

Note that adsorption in the empty pores is not modelled and liquid films are not accounted for. The hydraulic conductivity of thin liquid films that develop in cylindrical throats is so low that they have no significant contribution to mass transfer (Metzger et al., 2007c). We will consider pores of diameter 100 nm with a narrow distribution so that the reduction of vapour pressure due to the Kelvin effect is almost uniform for all pores and only about 2%. At atmospheric pressure, Knudsen effect in vapour diffusion only plays a significant effect if pore size is smaller than the chosen one (Kast, 1988). Therefore, we are neglecting both Kelvin and Knudsen effect.

Concerning the liquid-filled part of the network, random pore size distribution and capillary flow lead to irregular emptying of pores and the appearance of disconnected clusters. If

viscous (and gravity) effects are neglected, water flow within these liquid clusters is entirely controlled by capillary pressure differences so that (unlike in Fig. 1) *only the largest* meniscus throat of the cluster empties. The rate at which this happens is obtained by summing up the evaporation rates for all menisci of the respective cluster. This choice of largest meniscus and computation of the emptying rate is done for all clusters. At every moment during drying, the time step is given by complete emptying of *first* throat in the network since this will change liquid connectivity as well as the set of Eq. (1) for vapour diffusion. In this way, drying is described as a discrete process and the kinetics are given by a steady-state expression for vapour diffusion.

2.2. *Viscous model*

If liquid viscosity is accounted for, liquid flow rates depend on actual pressures $p_{w,i}$ and at each liquid pore node (black circles in Fig. 1) add up to zero as

$$\sum_j \dot{M}_{w,ij} = \sum_j \frac{\pi r_{ij}^4}{8\nu_w L_{ij}}(p_{w,i} - p_{w,j}) = 0 \qquad (2)$$

where ν_w is kinematic viscosity of water and L_{ij} liquid-filled length of pore throats. Boundary conditions to Eq. (2) are given at the menisci at the liquid–gas interface. For stationary menisci (in full throats where liquid can be provided at the local evaporation rate), the second kind boundary condition $\dot{M}_{w,ij} = \dot{M}_{v,ij}$ is applied. For moving menisci (in the largest throat of the cluster, in all partially filled throats and where liquid cannot be supplied at the local evaporation rate), the boundary condition of first kind $p_{w,j} = p - 2\sigma/r_{ij}$ (with surface tension σ and assuming perfect wetting of the liquid, i.e. zero contact angle) is used. Since choice of boundary conditions and flow rates are interdependent, iteration is used to determine the actual liquid flow field. The quasi-steady motion of menisci (now possibly several per cluster as in Fig. 1) is obtained as the difference between vapour and liquid flow, and the same principle of time stepping is applied as in the non-viscous case. (Note that, in the gas phase, viscosity is not modelled and constant pressure is assumed.)

Table 1 – Physical constants for simulation

Physical constant	Value
T (K)	293
p (Pa)	10^5
p_v^* (Pa)	2339
δ (mm^2/s)	25.69
σ (N/m)	0.072
ν_w (mm^2/s)	1.002

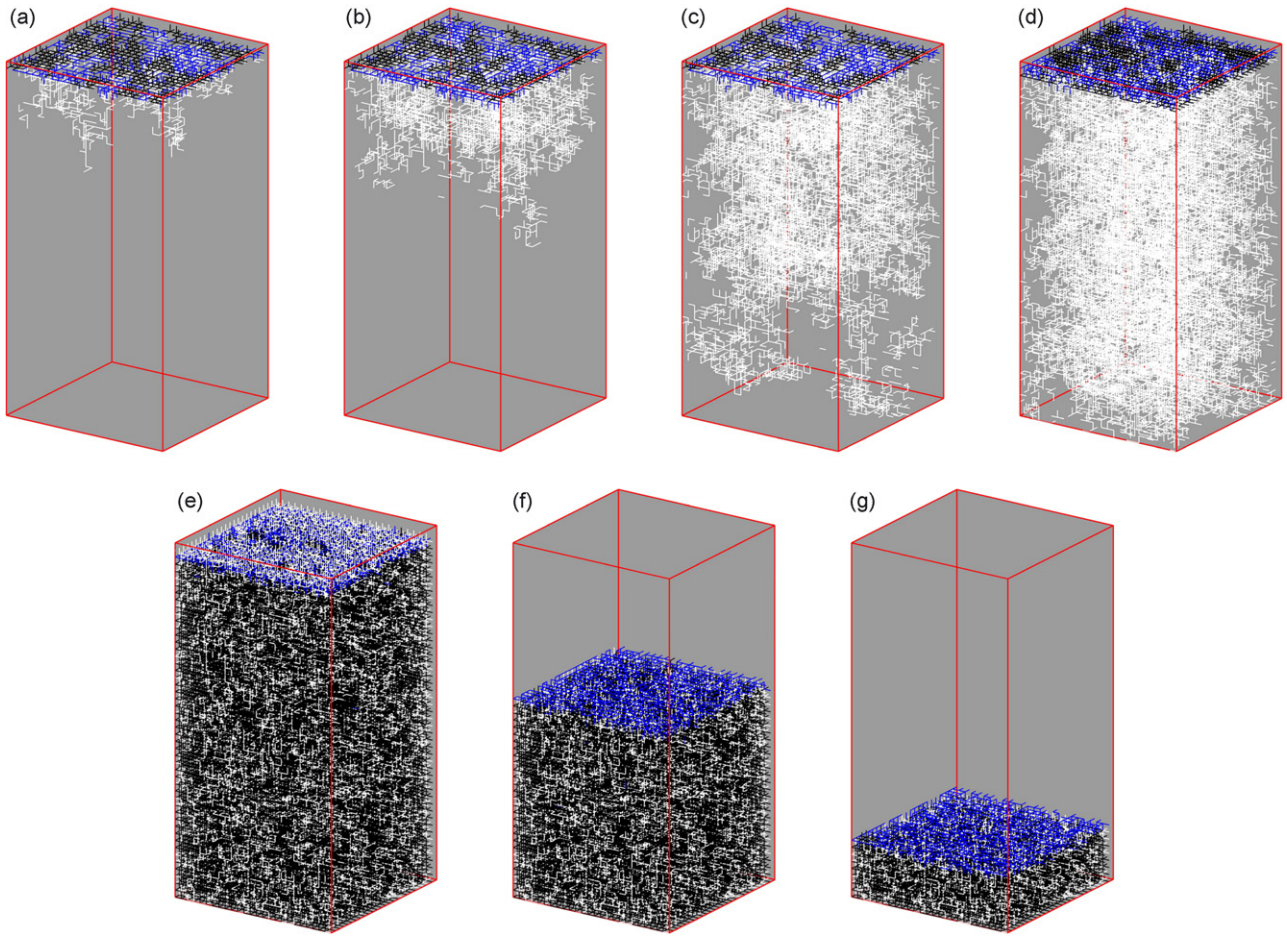

Fig. 2 – Phase distributions for *non-viscous* case at network saturations (a) 0.98; (b) 0.95; (c) 0.86; (d) 0.75; (e) 0.67; (f) 0.39; (g) 0.11; white lines represent empty throats, black is for liquid throats and blue for partially filled throats. The network is open for evaporation at the top; periodic boundary conditions are applied in horizontal directions. (For better readability, empty throats are not shown in top layers with an average saturation lower than 0.26; neither are full throats shown in bottom layers with an average saturation higher than 0.74.) (For interpretation of the references to colour in this figure legend, the reader is referred to the web version of the article.)

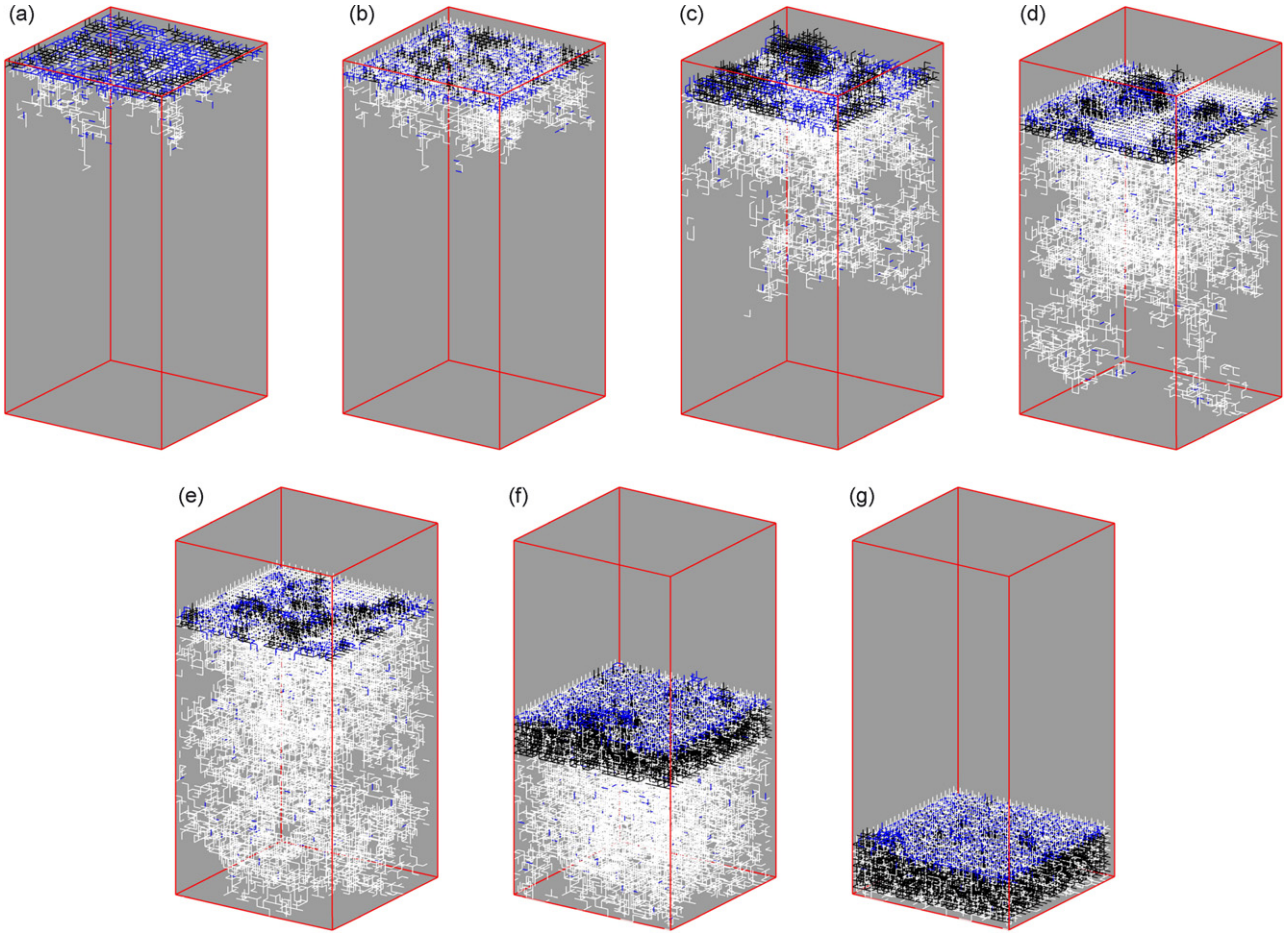

Fig. 3 – Phase distributions for *viscous* case at network saturations (a) 0.98; (b) 0.95; (c) 0.86; (d) 0.75; (e) 0.67; (f) 0.39; (g) 0.11; white lines represent empty throats, black is for liquid throats and blue for partially filled throats. The network is open for evaporation at the top; periodic boundary conditions are applied in horizontal directions. (For better readability, empty throats are not shown in top layers with an average saturation lower than 0.26; neither are full throats shown in bottom layers with an average saturation higher than 0.74.) (For interpretation of the references to colour in this figure legend, the reader is referred to the web version of the article.)

3. Simulation results

Present computational limitations impose a relatively small network size ($25 \times 25 \times 50$) so that rather unrealistic values have to be chosen for pore geometry and drying conditions to observe significant viscous effects. Air flow is at room temperature and atmospheric pressure and contains no moisture ($p_{v,\infty} = 0$); we consider water as a liquid (the physical constants for the simulation are given in Table 1); boundary layer is 50 μm thin, corresponding to a mass transfer coefficient $\beta = 0.51$ m/s and an initial drying rate of 9 g/m^2 s (for a completely wet surface). Throats have a very narrow radius distribution (50 ± 1 nm) and length 500 nm; this means that porosity is low (9.4%) and that only a thin near-surface region (depth 25 μm) of the porous medium is described. Effects sim-

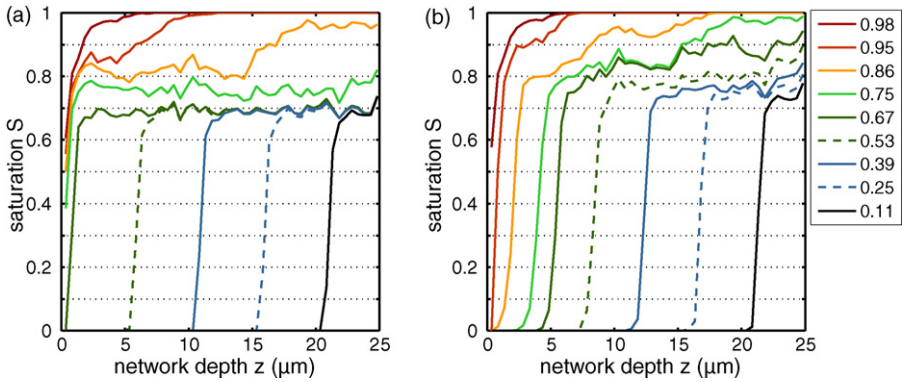

Fig. 4 – Profiles of slice-averaged saturation during drying: (a) non-viscous (b) viscous. (Solid lines correspond to the choice of phase distributions shown in Figs. 1 and 2.)

ilar to the ones discussed below will also occur for realistic conditions, but over longer distances.

Being interested in the role of liquid viscosity, drying of the same network is once simulated neglecting the viscous effects and once accounting for them. Respective phase distributions during drying are shown in Figs. 2 and 3; by slice averaging, they are converted into one-dimensional saturation profiles as plotted in Fig. 4. Corresponding drying rate curves are given in Fig. 5; the drying rate is put into dimensionless form by setting its initial value to unity.

If liquid viscosity is neglected, capillary pumping experiences no constraint as long as the liquid is connected over the whole network. During this period, no drying front occurs, but gas penetrates into the depth of the network and saturation level drops more or less uniformly throughout the network (Figs. 2a–d and 4a). Network surface stays sufficiently wet so that lateral vapour transfer in the gas-side boundary layer can ensure that liquid is evaporated at a constant rate (Fig. 5). At a critical saturation of about 0.7, the liquid phase has split up into small disconnected clusters, network surface dries out (Fig. 2e) and a receding evaporation front is observed (Figs. 2f and g and 4a). Drying rate drops due to the additional vapour transfer resistance in the network (Fig. 5). The mentioned critical saturation is expected to be lower for larger pore networks (Le Bray and Prat, 1999; Yiotis et al., 2006).

If viscous effects are modelled, they do not play a significant role in the very initial drying phase (here $S > 0.98$) which is still dominated by capillary forces (compare Figs. 2a and 3a). But as flow distances become longer and surface saturation decreases, differences in capillary pressure are not enough to supply liquid at the high local evaporation rates (which are even enhanced by lateral diffusion in the boundary layer). Therefore, all surface throats dry out (Fig. 4b) and a quite narrow drying front recedes into the pore network. As a consequence, drying rates are strongly reduced (Fig. 5), so that, as drying proceeds, this receding front can widen up gradually (Figs. 3c and d and 4b). In the viscous case, breakthrough occurs long after network surface is dry. Note also that the competition between menisci for liquid flow is documented by many moving menisci in one cluster (blue throats in Fig. 3).

With further decreasing drying rate, saturation gradient is reduced more and more (Fig. 4b) and local saturations approach the limit for liquid disconnection (Fig. 3e and f). In the final stages of drying, viscous effects play only a little role (compare Figs. 2g and 3g, see Fig. 5). This non-viscous limit ought to gain significance for deeper networks.

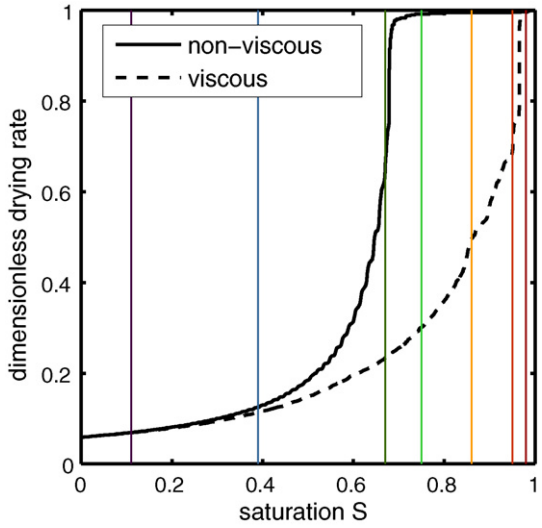

Fig. 5 – Drying rate curves for non-viscous and viscous case. (Vertical lines correspond to the choice of network saturations in the other figures.)

If we consider a characteristic length over which liquid can be pumped at a given available capillary driving force (Metzger et al., 2007c), this is found to be inversely proportional to drying rate and – neglecting vapour transfer resistance in the boundary layer – proportional to the thickness of the dried layer of the pore network. Therefore, the drying front can widen up with no upper bound if the network is arbitrarily deep, unlike in the gravity-stabilized case where front width fluctuates around a *constant* value.

Note that one of our assumptions has been perfect wetting of the liquid; for contact angles greater than zero the capillary pressures at the menisci will be less pronounced as well as the available pressure differences for driving capillary flow. This means that we have taken the minimum ratio of viscous to capillary effects; viscosity may still play a role if the pore size distribution is chosen slightly wider.

Conclusions

We have observed that viscous effects play a major role in the intermediate stages of drying whereas short- and long-time drying behaviour are similar to the non-viscous case. The relative size of viscous effects is decisive for phase distributions and drying rates in these intermediate stages of the drying process – and will especially determine the duration of the constant drying rate period. For our specific case, we observed a near-disappearance of this period whereas in many real porous media it is of considerable importance. The reason is that we have chosen a very narrow pore size distribution. Two-dimensional simulations for more realistic cases of pore size distributions – wider or even bimodal ones – show little effect of liquid viscosity (Metzger et al., 2007a).

Future work shall further investigate the local variation of saturation in the drying front and the scaling behaviour of its width with capillary number as already studied by Prat and Bouleux (1999). This shall pave the way to describe drying behaviour of much larger porous structures.

In the same context, a continuous model will be assessed that accounts for vapour diffusion in a dry zone and for viscous flow in the partially saturated zone driven by differences in capillary pressure (described by the generalized Darcy law). To this purpose, effective model parameters, such as liquid permeability and capillary pressure, will first be computed from the phase distributions as observed in a drying pore network (described by the above viscous model); then, saturation profiles shall be computed by the continuous model and compared to the profiles obtained from network simulations (as in Fig. 4b).

REFERENCES

Huinink, H.P., Pel, L., Michels, M.A.J. and Prat, M., 2002, Drying processes in the presence of temperature gradients. Pore-scale modelling. Eur Phys J E, 9: 487–498.

Kast, W., (1988). *Adsorption aus der Gasphase*. (VCH, Weinheim).

Laurindo, J.B. and Prat, M., 1996, Numerical and experimental network study of evaporation in capillary porous media. Phase distributions. Chem Eng Sci, 51: 5171–5185.

Laurindo, J.B. and Prat, M., 1998, Numerical and experimental network study of evaporation in capillary porous media. Drying rates. Chem Eng Sci, 53: 2257–2269.

Le Bray, Y. and Prat, M., 1999, Three dimensional pore network simulation of drying in capillary porous media. Int J Heat Mass Transfer, 42: 4207–4224.

Metzger, T., Irawan, A. and Tsotsas, E., 2007, Isothermal drying of pore networks: influence of friction for different pore structures. Dry Technol, 25: 49–57.

Metzger, T., Irawan, A. and Tsotsas, E., 2007, Influence of pore structure on drying kinetics: a pore network study. AIChE J, 53: 3029–3041.

Metzger, T., Tsotsas, E. and Prat, M., 2007, Chapter 2—Pore-network models: a powerful tool to study drying at the pore level and understand the influence of structure on drying kinetics, in Modern Drying Technology, Vol. 1, Computational Tools at Different Scales, Tsotsas, E. and Mujumdar, A.S., Mujumdar, A.S. (eds) (Wiley-VCH, Weinheim, Germany), pp. 57–102.

Nowicki, S.C., Davis, H.T. and Scriven, L.E., 1992, Microscopic determination of transport parameters in drying porous media. Dry Technol, 10: 925–946.

Plourde, F. and Prat, M., 2003, Pore network simulations of drying of capillary media. Influence of thermal gradients. Int J Heat Mass Transfer, 46: 1293–1307.

Prat, M., 1993, Percolation model of drying under isothermal conditions in porous media. Int J Multiphase Flow, 19: 691–704.

Prat, M. and Bouleux, F., 1999, Drying of capillary porous media with stabilized front in two-dimensions. Phys Rev E, 60: 5647–5656.

Prat, M., 2007, On the influence of pore shape, contact angle and film flows on drying of capillary porous media. Int J Heat Mass Transfer, 50: 1455–1468.

Segura, L.A. and Toledo, P.G., 2005, Pore-level modeling of isothermal drying of pore networks. Effects of gravity and pore shape and size distributions on saturation and transport parameters. Chem Eng J, 111: 237–252.

Shaw, T.M., 1987, Drying as an immiscible displacement process with fluid counterflow. Phys Rev Lett, 59: 1671–1674.

Tsimpanogiannis, I.N., Yortsos, Y.C., Poulou, S., Kanellopoulos, N. and Stubos, A.K., 1999, Scaling theory of drying in porous media. Phys Rev E, 59: 4353–4365.

Yiotis, A.G., Stubos, A.K., Boudouvis, A.G. and Yortsos, Y.C., 2001, A 2-D pore-network model of the drying of single-component liquids in porous media. Adv Water Resour, 24: 439–460.

Yiotis, A.G., Boudouvis, A.G., Stubos, A.K., Tsimpanogiannis, I.N. and Yortsos, Y.C., 2003, Effect of liquid films on the isothermal drying of porous media. Phys Rev E, 68: 037303-1–037303-4.

Yiotis, A.G., Boudouvis, A.G., Stubos, A.K., Tsimpanogiannis, I.N. and Yortsos, Y.C., 2004, The effect of liquid films on the drying of porous media. AIChE J, 50: 2721–2737.

Yiotis, A.G., Tsimpanogiannis, I.N., Stubos, A.K. and Yortsos, Y.C., 2006, Pore-network study of the characteristic periods in the drying of porous materials. J Colloid Interface Sci, 297: 738–748.